Instrument intercomparison in the pulsed neutron fieldsat the CERN HiRadMat facility

E. Aza [a,b], M. Caresana [c], C. Cassell [c,d], N. Charitonidis [a,e], E. Harrouch [a], G.P. Manessi [a,f,*], M. Pangallo [a], D. Perrin [a], E. Samara [a,g], M. Silari [a]

[a] CERN, CH-1211 Geneva 23, Switzerland
[b] Aristotle University of Thessaloniki, Department of Physics, GR-54124 Thessaloniki, Greece
[c] Politecnico of Milan, Department of Energy, Via Ponzio 34/3, IT-20133 Milan, Italy
[d] University of Wollongong, Centre for Medical Radiation Physics, NSW 2522, Australia
[e] École Polytechnique Fédérale de Lausanne, Particle Accelerator Physics Laboratory, CH-1015 Lausanne, Switzerland
[f] University of Liverpool, Department of Physics, L69 7ZE Liverpool, UK
[g] University of Athens, Department of Physics, GR-15771 Athens, Greece

Received 11 June 2013
Received in revised form
3 December 2013
Accepted 22 December 2013

1. Introduction

In the last decades radiation protection has been dealing with an increasing number of applications where PNF[1] represent an important component of the stray radiation field, e.g. around particle accelerator facilities, plasma wake field accelerators and free electron laser facilities. It is well known that active neutron detectors can suffer severe limitations when used in these operating conditions. The limitations are due to electronics constraints, i.e. the finite resolutions of the counting system (dead time effects when counting high reaction rates) and physical reasons, e.g. the diminution of the gas multiplication factor of proportional counters during the detection of a neutron burst (Rios et al., 2013) and volume recombination effects for ionization chambers. A comprehensive study focused on the evaluation of the behaviour of 14

* Corresponding author. CERN, CH-1211 Geneva 23, Switzerland.
E-mail address: giacomo.paolo.manessi@cern.ch (G.P. Manessi).

[1] PNF = Pulsed Neutron Fields.

neutron area monitors and 15 personal dosemeters in PNF has been recently carried out by Caresana et al., 2014.

This paper presents and discusses the results of a similar experiment conducted at the High Radiation to Materials (HiRadMat) facility at CERN (Efthymiopoulos et al., 2011), with a different set of detectors and under different conditions. The aim was to verify the response linearity of several neutron detectors in extreme pulsed conditions as a function of the neutron burst intensity. In fact, as stated in Caresana et al. (2013a), two of the four requirements for an ideal detector to be used in PNF are the capability to withstand very high instantaneous neutron fluxes with little or no saturation and, at the same time, to correctly measure the intensity of a single neutron burst. This makes the response linearity a fundamental parameter in determining the suitability of a detector for use in PNF, as it quantifies its ability to meet these two requirements.

Five detectors were employed: a novel rem counter specifically conceived for applications in PNF, called LUPIN (Long-Interval, Ultra-wide dynamic, PIle-up free Neutron rem counter) (Caresana et al., 2013a,b; Ferrarini et al., 2010), two commercial rem counters (a Thermo Scientific FHT 762 Wendi-2 and a FHT 752 BIOREM) and two ionization chambers (pressurised Argon and Hydrogen type) employed in the Radiation Monitoring System for Environment and Safety (RAMSES) (Segura Millan et al., 2006) at CERN. Since most of the monitoring stations at CERN usually deal with pulsed stray fields, this experiment was also conceived to verify the performance of the RAMSES detectors in extreme conditions.

The measurements were performed in the new HiRadMat facility at CERN. The facility has been specially designed for conducting experiments in order to investigate the effects of high intensity pulsed radiation on materials. The detectors were exposed in the stray field generated by a proton beam of very short duration with momentum of 440 GeV/c impinging on the dump. The secondary neutrons produced in the dump scatter through a 50 m long concrete tunnel before reaching the detectors. In order to intercompare the detectors in five different positions a specially designed, remotely controlled, rotating support was designed and built.

The beam intensity could be altered by changing the number of pulses in the proton bunch, while preserving the beam structure. This allowed the detectors to be comprehensively tested up to extreme stray field intensities, and the non-linear aspects of their response analysed. The beam intensity was steadily increased during the experiment by more than three orders of magnitude, with an H*(10) due to neutrons varying between a few nSv/burst and a few μSv/burst. As a consequence of the neutron scattering on the concrete walls and the tunnel structures, the stray field at the detector positions contains a significant delayed neutron component. This allowed the detector response to be tested in a pulsed stray field, in which a slow contribution is also observed.

2. Materials and methods

2.1. The HiRadMat facility

HiRadMat is a newly constructed facility designed to provide high-intensity pulsed beams to an irradiation area where beam-to-material experiments can be performed. The facility has been constructed 35 m under the ground level at the already existing tunnel of the old CERN WANF Area (Astier et al., 2003). The primary proton beam that reaches the irradiation area is extracted from the Super Proton Synchrotron (SPS). The nominal proton momentum is 440 GeV/c. The pulse consists of several bunches (from 1 up to 288, according to the user needs). The intensity of each bunch can be varied from 10^9 up to $1.7 \cdot 10^{11}$ protons and the spacing between them from 25 ns up to 100 ns. That gives a maximum pulse intensity of $5 \cdot 10^{13}$ protons/spill and a maximum pulse length of 28.8 μs. One pulse per SPS cycle (approximately 48 s) can be extracted. The available beam line optics allow for a flexible spot size from 0.5 mm^2 up to 2 mm^2. A layout of the experimental area is shown in Fig. 1, alongside with the code names of the tunnels.

For the purposes of this experiment, the proton beam was impinging directly on the beam dump, while the detectors were placed in the TA7 tunnel, just after the air-tight ventilation door that separates the experimental area from the access area. The HiRadMat beam dump (Grenier and Pardons, 2011) consists of a cylindrical graphite core of a diameter of 8 cm and total length of 350 cm. The core is enclosed into a larger cylindrical case, made from a special alloy (97% Al, 2% Cu, 0.4 Zn, 0.35% Cr), with a diameter of 16 cm and a length of 350 cm. This case is further enclosed into a cylindrical copper case with the same length and a diameter of 32 cm. The structure is surrounded by blocks of marble, iron and stainless steel. In addition, in order to completely stop the charged particles (produced in the dump core) from contaminating the rest of the tunnel, additional 10.5 m of iron blocks are placed behind the dump.

A beam spot size of around 2 $mm^2$and a bunch spacing of 50 ns were chosen. A list of the nominal intensities of the pulses to be extracted from the SPS and shot on the beam dump is shown in Table 1. These are the nominal values, while during the measurements the obtained intensities were slightly different and, in some cases some settings had to be skipped. An indication of the expected H*(10) per burst in the measuring area is also given, as obtained in a test run carried out before the main series of measurements (Charitonidis et al., 2012). The beam intensity is measured via a monitor affected by a 3% uncertainty.

2.2. The detectors

2.2.1. LUPIN

The LUPIN is a prototype extended range rem counter available in two versions, using either a ^{3}He or BF_3 proportional counter. The counter is inserted in a spherical or cylindrical moderator with lead and cadmium inserts and uses front-end electronics based on a logarithmic amplifier. The working principle is simple: the current generated inside the proportional counter is amplified with a current to voltage logarithmic amplifier and the output voltage is acquired with an Analog to Digital Converter (ADC). The current is integrated over a user settable time window. The integrated charge divided by the charge expected by a single neutron interaction gives the number of neutrons occurring in a defined time. The output value in H*(10) is obtained by applying a proper calibration factor, expressed in nSv/interaction. The cylindrical BF_3 version was employed for this experiment. The calibration, carried out in the CERN laboratory with a ^{238}PuBe source with activity of 1.85 TBq, gave factor of 0.480 nSv/interaction.

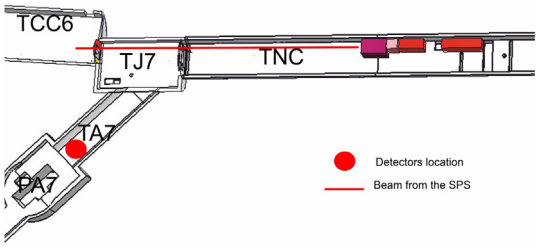

Fig. 1. Layout of the HiRadMat facility. The beam (black line) was impinging on the dump in the TNC tunnel, while the detectors were placed in the TA7 tunnel (red spot). (For interpretation of the references to colour in this figure legend, the reader is referred to the web version of this article.)

Table 1
Nominal beam settings used during the experiment.

Setting number	Pulse intensity [protons on dump]	Expected H*(10) per burst
1	$5\cdot10^{9}$	2.5–5 nSv
2	10^{10}	5–10 nSv
3	$2\cdot10^{10}$	10–20 nSv
4	$4\cdot10^{10}$	20–40 nSv
5	$7.5\cdot10^{10}$	37.5–75 nSv
6	10^{11}	50–100 nSv
7	$2\cdot10^{11}$	100–200 nSv
8	$4\cdot10^{11}$	200–400 nSv
9	$7.5\cdot10^{11}$	375–750 nSv
10	10^{12}	500–1000 nSv
11	$2\cdot10^{12}$	1000–2000 nSv
12	$4\cdot10^{12}$	2000–4000 nSv
13	$7.5\cdot10^{12}$	3750–7500 nSv

2.2.2. Thermo Scientific FHT 752 (BIOREM)

The Thermo Scientific FHT 752 BIOREM is a commercial neutron dose rate metre for stationary and portable use, especially suited for environmental measurements. It employs a BF_3 proportional counter placed in a cylindrical moderator containing polyethylene and boron carbide. The output is given in H*(10), but an internal calibration factor, expressed in nSv/count, can be set by the user. The calibration carried out at CERN resulted in a calibration factor of 0.550 nSv/count.

2.2.3. Thermo Scientific FHT 762 (Wendi-2)

The Thermo Scientific FHT 762 Wide Energy Neutron Detection Instrument (Wendi-2) is a commercial extended range rem counter designed to measure the H*(10) rate within an energy range from thermal up to 5 GeV (Jägerhofer et al., 2012). It consists of a ^{3}He proportional counter surrounded by a cylindrical polyethylene moderator assembly and a layer of tungsten powder. This additional layer of high-Z material enhances the detector response to high-energy neutrons via inelastic scattering interactions (Olsher and McLean 2008; Olsher et al., 2000). The output is given in H*(10), but the internal calibration factor can be changed by the user. The calibration carried out at CERN resulted in a calibration factor of 0.320 nSv/count.

2.2.4. Argon and hydrogen-filled ionization chamber

The gas-filled ionization chambers used for RAMSES are customised Centronic IG5-H20. Designed for use in mixed radiation fields, they are capable of detecting high-energy charged particles, photons and neutrons. The gas is pressurised to 20 bars ($2\cdot10^{6}$ Pa). The energy range is 50 keV up to 10 MeV and the measuring range is100 nSv/h up to 10 Sv/h (Theis 2007). A charge digitizer converts the charge created in the active volume to TTL pulses, which can be collected by digital data acquisition cards. To convert the output signal into H*(10), a calibration factor, expressed in nSv/pC or nSv/count, must be applied. This is calculated for each monitoring station according to the expected neutron and gamma spectra in the area. The calculation is done by folding the response function of the detectors (see Theis et al., 2004) with the spectra known experimentally or simulated.

2.3. Experimental set up

The detectors were tested at the end of the TA7 tunnel (see Fig. 1). In this area the stray radiation field is only due to neutrons because it is at a distance of 50 m from the dump and the photon component is strongly attenuated, while the neutrons scatter towards the wall and the floor of the tunnel. In a test run carried out before the main series of measurements, it was verified that the radiation gradient in the area is quite high (30% difference in the measured H*(10) between two positions 2 m from one another (Charitonidis et al., 2012)). Due to the radiation gradient, and given the difficulty to access the measurement area, it was decided to build a rotating support for the five detectors that could be remotely controlled. This solution allowed testing each detector in 5 positions, so as to have a comparison of the responses in the same conditions of stray field with good reproducibility. Moreover, since no access to the experimental area is allowed when SPS is filling the LHC, the number of accesses had to be limited. With this solution the accesses to the area were limited to one before the experiment in order to install the equipment and one after the measurements for dismantling.

2.3.1. The rotating support

The support has been designed in the form of a Ferris wheel, with five supports, each one attached to the skeleton in such a way that, as the wheel turns, the supports are kept upright by gravity. The skeleton is welded onto a central axis. This axis is supported by two vertical beams that are welded on a base plate, mounted for stability on two horizontal beams. The support was entirely built out of aluminium to minimize the total weight as well as to limit activation issues. A rotary motor makes the entire assembly rotate with a transmission belt while an encoder gives information on the absolute angular position (Charitonidis and Harrouch, 2013). The overall set-up could be checked on-line via awe camera installed next to the wheel. The distance between the five supports was maximized (being limited by the height of the tunnel ceiling) in order to reduce cross-interferences between the detectors. The configuration scheme and a picture with the detectors mounted on the wheel are shown in Fig. 2.

2.4. Data acquisition

The data acquisition for the four detectors used in RAMSES was carried out according to the standard procedure that is followed for all the CERN monitoring stations. The data from the detectors is gathered every second in a local electronics station, which processes and sends them via an Ethernet connection, available in the experimental area, to the central server. The data is afterwards retrieved for the off-line analysis from the RAMSES database. The time was synchronised during the measurements with the server time and recorded. Both the detectors and the local station were connected to a power supply.

The signal of the LUPIN was partially processed by the front-end electronics (internally powered by a battery) and then output to a

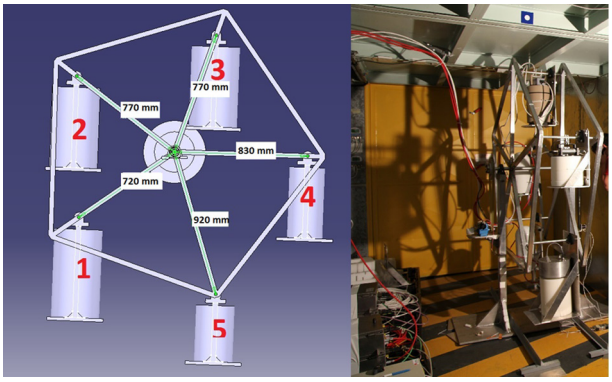

Fig. 2. Technical Drawing (left) and photograph (right) of the rotating support installed in the facility. The arbitrary numbers given to identify the positions are also shown.

Bayonet Neill Concelman (BNC) cable. A custom made cable allowed for the signal to be delivered to the HiRadMat control room on the surface, where the output was connected to a Personal Computer (PC) oscilloscope (PicoScope 4424 by PicoTechnology), which in turn was connected to a portable computer. The data was monitored on-line by a LabVIEW® program, acquired at a frequency of 5 MHz and stored on log-files for the off-line analysis.

3. Results

3.1. FLUKA simulations

Monte Carlo simulations were carried out with the FLUKA code (Battistoni et al., 2007; Fasso et al., 2005) (version 2012.2.17) to calculate the neutron energy distributions at the end of the TA7 tunnel, where the detectors were installed. A detailed geometry model of the tunnel civil engineering structures, the beam dump and the basic electromechanical equipment of the HiRadMat access and experimental area (Charitonidis et al., 2011) were implemented in FLUKA, together with the neutron detectors. The primary proton beam, with a nominal momentum of 440 GeV/c and a Gaussian shape with a spot size of 2 mm, was simulated to impinge on the dump. Since the dump core consists of 350 cm of graphite, whose nuclear interaction length is 38.8 cm, all the protons interact with the graphite, producing a hadronic cascade and an electromagnetic shower. The simulated prompt neutron spectrum produced at the dump, which is backscattered towards TJ7, was scored 2 m upstream of the dump core (Fig. 3).

The neutron spectrum consists of five components: a thermal part, due to neutron elastic scattering interactions on the iron and marble structures of the dump as well as on the concrete walls of the tunnel; an intermediate region from 10 eV up to 1 MeV; an evaporation component, caused by the particle-nucleus quasi-elastic interactions with most probable energy in the MeV region; a high energy component (>10 MeV) due to particle-nucleon high-energy interactions. Because the p−n cross section of most shielding materials (like iron and concrete) reaches a minimum at about 100 MeV, the appearance of this Maxwellian-shaped high-energy peak occurs in our case around this energy value. Finally, the very high energy part (>10 GeV) comes from the backscattering of high energy neutrons produced inside the dump.

The thermal and evaporation neutrons are dominating the spectrum, while the high energy component is around three orders of magnitude lower. In fact high energy neutrons produced in the dump are mainly forward peaked, while only a very small portion is backscattered at 180°. These backscattered neutrons continue travelling and scattering through the TNC, TJ7 and TA7 tunnels. The simulated neutron spectra that finally reach the detectors are shown in Fig. 4.

The shape of the neutron spectrum reaching the detectors is significantly different from the one produced near the dump. The thermal component is the one that dominates the neutron spectral fluence, since the intermediate and high energy neutrons produced in the dump are backscattered on the tunnels floor and walls for 50 m (total distance between the detectors and the beam dump). Therefore, a significant portion of the intermediate energy neutrons (from tens of eV up to a few hundred keV) produced in the dump loses a significant part of their energy. Additionally, since the TA7 tunnel has an angle of 45° with respect to TNC, the majority of the backscattered intermediate and high-energy neutrons from the beam dump follow a straight course and escape through the TJ7 and TCC6 tunnels (see Fig. 1). This accounts for the decrease of about six orders of magnitude in the total number of neutrons between the position near the dump and the detector positions. At the same time, this explains the strong reduction of the evaporation peak at about 1 MeV (which is instead clear in Fig. 3). The statistical uncertainties for energies higher than 1 MeV are quite high, since the number of neutrons reaching the detectors in this energy region is very limited.

The arrival time distribution of the neutrons at the detector reference positions was also simulated. The results are shown in Fig. 5. The distribution is divided in four parts according to the neutron energy.

As expected, the high energy component of the field (i.e. the one with the higher velocity) is the first which is reaching the detectors. The last neutrons arrive about 100 ms after the beam impinged on the dump.

3.2. Detector calibrations

Since the aim of the experiment is to check the linearity of the response of the detectors, the focus is not on the match between the simulated values of H*(10) per primary and the measured ones. Nevertheless, it was decided, when possible, to set the calibration factor of the detector taking into account the expected neutron spectra and the H*(10) per primary as simulated via FLUKA in the five measuring positions. The process followed to set the proper calibration factor is explained below for each detector.

Where the folding between the response function of the detector and the simulated spectrum was not possible, the calibration

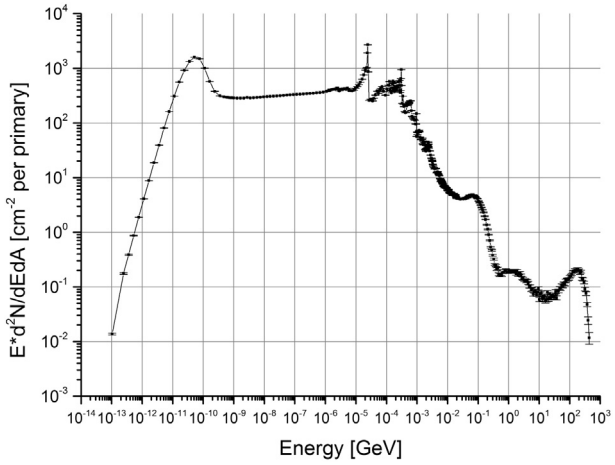

Fig. 3. Simulated backscattered neutron spectrum at 2 m upstream of the beam dump, in isolethargic view. The results are normalized per primary proton.

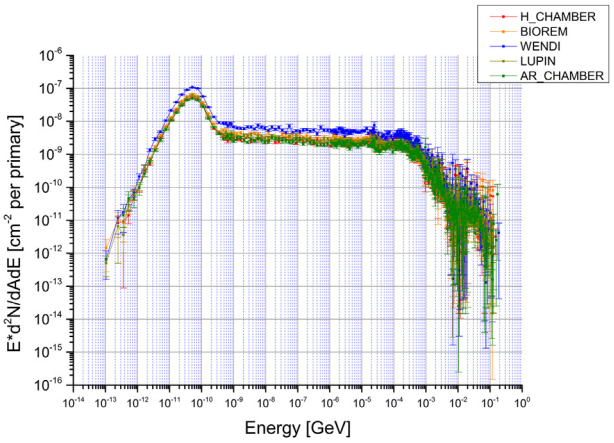

Fig. 4. The simulated neutron spectra at each of the detector reference positions. The plot is in isolethargic view. The results are normalized per primary proton.

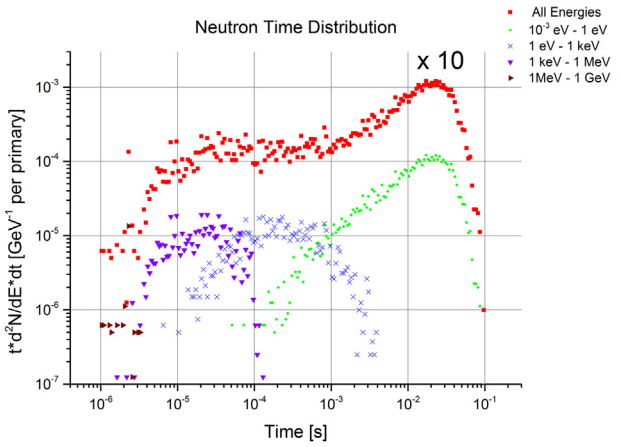

Fig. 5. The simulated time distribution of the neutrons at the detector reference positions. The red, blue, green and brown plots represent the low, medium, high and very high energy components, respectively. The black plot, differently scaled for better visualization, is the sum of all the components. The beam impinges on the dump at $t = 0$. (For interpretation of the references to colour in this figure legend, the reader is referred to the web version of this article.)

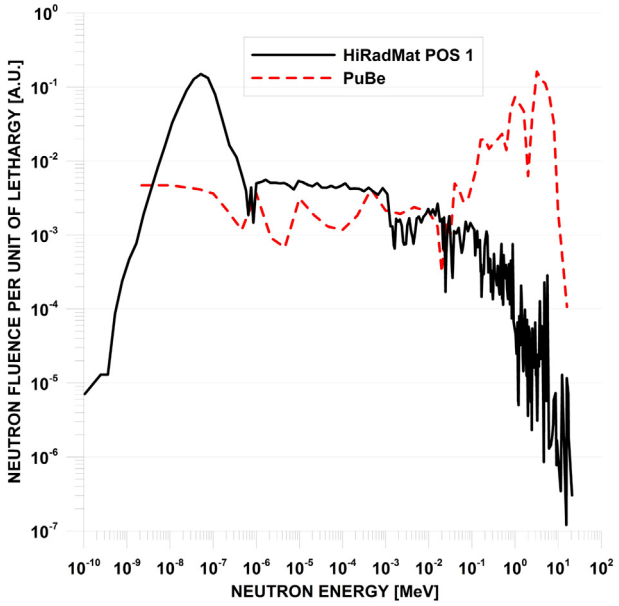

Fig. 6. Comparison of the neutron spectrum of the ^{238}PuBe source of the CERN calibration laboratory and the one expected in HiRadMat measuring position 1. The spectra have been normalized (integrated area below the spectra equal to 1) and are given in arbitrary units.

factor obtained in the CERN laboratory with the ^{238}PuBe source was kept. It should be noted that this value is affected by an uncertainty of 7%, as reported in the calibration certificate of the source. At the same time, where the folding was possible, the calculated factors are affected by two contributions of uncertainty: the first on the response function, the second on the simulated spectrum, both calculated via Monte Carlo codes. However, it was decided not to take into account any kind of uncertainty for two reasons: firstly, because these are correlated uncertainties, which are the same for all the detectors (in fact all of them were calibrated with the same source and/or folded with the same simulated neutron spectra); secondly, because this would not have improved the check of the response linearity.

3.2.1. LUPIN

Since the response function of the detector is still known only in arbitrary units (the detector is under characterization) and for a limited number of energies (see Aza et al., 2013), it was decided to use the ^{238}PuBe calibration factor determined in the CERN calibration laboratory. However, the simulated spectral fluence is slightly different from the ^{238}PuBe one, being characterized by a peak at thermal energy and a rapid drop for energies higher than 100 keV. A comparison of the two spectra is shown in Fig. 6.

3.2.2. BIOREM FHT 752

The response function of the detector is known in units relative to the response of a source of moderated ^{252}Cf. However the sensitivity of the detector to this neutron field is unknown and the response function itself is not accurately known for thermal energies, i.e. where the simulated spectra have a huge peak. Therefore it was decided not to modify the calibration factor obtained with the ^{238}PuBe source.

3.2.3. Wendi-2

For the Wendi-2 the response function is well known for the entire neutron energy spectrum. This function was folded with the simulated neutron spectrum for each measuring position to derive the expected number of counts per primary. The expected value of H*(10) per primary (expressed in nSv/primary) simulated via FLUKA was then employed to obtain the best calibration factor to be used (nSv/count). However, this value has been found to be equal in all the positions to the one obtained in the calibration laboratory, i.e. 0.32 nSv/count.

3.2.4. Hydrogen and argon-filled ionization chamber

For both RAMSES ionization chambers the response function to neutrons is well known. Therefore the same procedure used to derive the Wendi-2 calibration factor was used, except for the fact that the values are expressed in terms of unit of charge and not counts. The results for the five positions are given in Table 2.

3.3. Detector data

The results of the measurements are shown for position 1 in Fig. 7. This position is representative of all the others, since the results obtained in positions 2–5 were very similar to those obtained in position 1 (full results are given. in ref. (Aza et al., 2013). The lines fitting the experimental data points are compared with a straight line that represents the bisector of the first quadrant, i.e. the ideal linear response. The equation used to fit the data were chosen only as visual guides and are power polynomials of the form $y = A \cdot x^B$. The measured values refer to the integrated H*(10) detected in the stray field generated by a single beam pulse impinging on the dump.

The uncertainty corresponds to the statistical one for the LUPIN, the BIOREM and the Wendi-2. For the ionization chambers (for which it is not possible to derive a statistical uncertainty) the global uncertainty has been set equal to 1%: this includes possible changes

Table 2
Calibration factors used for the RAMSES Hydrogen-filled and Argon-filled ionization chambers in the five measuring positions. All the values are in nSv/pC.

Position 1	Position 2	Position 3	Position 4	Position 5
Hydrogen-filled ionization chamber				
3.77	3.85	3.81	3.76	3.78
Argon-filled ionization chamber				
6.52	6.61	6.62	6.24	6.44

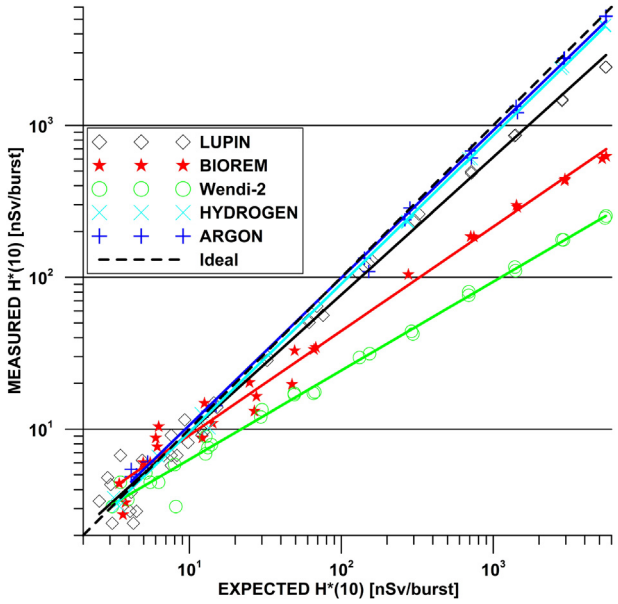

Fig. 7. Response of the detectors in position 1. The dotted line is the bisector of the first quadrant, representing the ideal linear behaviour. The uncertainties are not shown for clarity.

in the gas sensitivity due to variation in the temperature during the experiment and minor uncertainties on the electronic components of the analysing circuit as given by the manufacturer (Latu 2007). Since the aim of the experiment was to check the response linearity, the uncertainty on the positioning was neglected. In fact this would have affected only the comparison between data acquired with different detectors in the same position. The expected H*(10) was calculated by applying to the beam intensity a coefficient, expressed in nSv per proton on dump, derived from the linear region of the LUPIN and the two ionization chambers, i.e. at low beam intensities, where saturation effects are not present. The coefficients used for the five positions are given in Table 3.The values of expected H*(10) are affected by two sources of uncertainties: 3% derived from the uncertainty on the beam intensity; 5% due to the uncertainty on the coefficients.

4. Discussion

The response function is linear essentially over the entire H*(10) range for the Ar and H-filled chambers, with a slight underestimation only for values of expected H*(10) per burst higher than 1 μSv. For the other detectors the response is linear for low values of expected H*(10) and starts to saturate at higher intensities. The deviation from the ideal line is limited for the LUPIN, while it is of great importance for the BIOREM and the Wendi-2. Table 4 shows the ratios between the measured and the expected H*(10) averaged overall the positions for different values of expected H*(10) per burst. The ratios are not shown for values lower than 100 nSv/burst since the statistical uncertainties are too high to obtain a univocal value.

The underestimation of the expected H*(10) is lower than 5% for the Ar-filled chamber and 15% for the H-filled chamber over the entire intensity range. The underestimation of the LUPIN is acceptable (<30%) for expected H*(10) up to1 μSv/burst, while for the BIOREM and the Wendi-2 it is already very important for 100 nSv/burst (underestimation of a factor of 2 for the BIOREM, or a factor of 4 for the Wendi-2). At higher values of expected H*(10) the underestimation becomes of almost one order of magnitude for the BIOREM and the Wendi-2 that cannot therefore be considered reliable anymore, whereas for the LUPIN it is limited to a factor of 2.

Table 4
Ratio measured/expected H*(10) per burst for different values of expected H*(10) per burst.

Detector	Expected H*(10) per burst					
	100 nSv	200 nSv	500 nSv	1 μSv	2 μSv	5 μSv
LUPIN	0.76	0.75	0.73	0.68	0.57	0.45
BIOREM	0.51	0.36	0.26	0.22	0.16	0.12
Wendi-2	0.25	0.20	0.13	0.10	0.07	0.05
H chamber	0.90	0.89	0.89	0.87	0.86	0.85
Ar chamber	1.00	0.98	0.97	0.97	0.97	0.96

The underestimation of the H*(10) is due to both electronics and physical reasons. The former comes from the fact that the instruments working in pulse mode (like the BIOREM and the Wendi-2) are affected by dead time losses, that can become rather severe when high counting rates are encountered, which is the case when detecting PNF. Dead time corrections can be applied by internal algorithms to try to compensate for the losses, but these algorithms operate properly in steady-state radiation fields, whereas their reliability is low when dealing with pulsed fields of unknown time structure and H*(10) in the burst. To derive the dead time for each detector, which is not known *a priori* and is dependent on unknown limiting properties of the counting system, the "two-source method" (Knoll 2010) was applied to the acquired data. The obtained values are: (1.02 ± 0.10) μs for the BIOREM (very close to the TTL pulse width declared by the manufacturer, 1.2 μs (Thermo, 2008)) and (1.74 ± 0.17) μs for the Wendi-2. Forth LUPIN and the ionization chambers the calculation of the dead time would not have any physical meaning: in fact the LUPIN is not operating in pulse mode and the nature of the output pulses of the ionization chambers depends only on the characteristics of the digitizing circuit. It is clear from the derived values that the dead time losses are high for the BIOREM and the Wendi-2, whereas they are much lower for the two ionization chambers. This confirms the different level of underestimation noticed from the detector results.

The first physical reason explaining the detector underestimation regards proportional counters that use the integration of the total electric charge as a measure of the amount of the neutron signal, which is the case of the LUPIN. The underestimation comes from the diminution of the gas multiplication factor in the counter due to the shielding of the electric field, which is caused by accumulation of slow moving positive ions left behind by the multiplication process. This effect appears when neutrons interact with the detector during a time too short for the process of positive charge recollection (Rios et al., 2013).

A second physical reason explains the slight underestimation of the two ionization chambers. This is due to the incomplete ion collection caused by volume recombination, initial recombination and ion loss due to diffusion of ions to the collecting plates against the charge separating field. Among these processes only the losses due to volume recombination vary with the measured H*(10)

Table 3
Coefficients derived from the linear region of the LUPIN, H-filled and Ar-filled chambers, expressed for each position in nSv per proton on dump, with the related uncertainties.

Position 1	Position 2	Position 3	Position 4	Position 5
$(8.71 \pm 0.44)\cdot 10^{-10}$	$(5.37 \pm 0.27)\cdot 10^{-10}$	$(5.13 \pm 0.26)\cdot 10^{-10}$	$(6.90 \pm 0.35)\cdot 10^{-10}$	$(8.06 \pm 0.40)\cdot 10^{-10}$

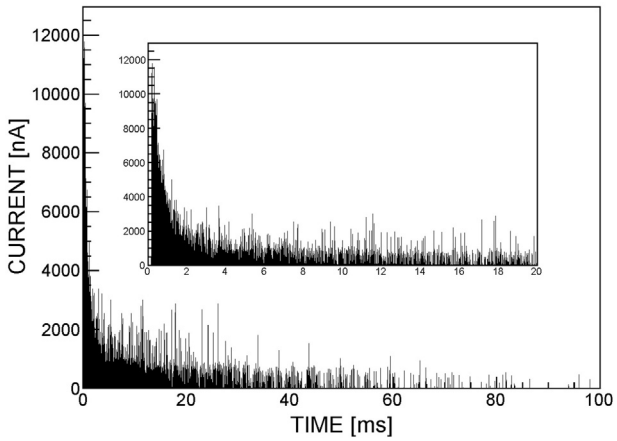

Fig. 8. Signal acquired with the LUPIN at beam setting 13 with an acquisition window of 100 ms. The insert is an expanded view of the first 20 ms window.

(Bohm 1976). This is taken into account by the manufacturer, which declares a possible maximum underestimation of the H*(10) of 15% when the ionization chambers are dealing with a charge per pulse in the order of tens of nC, i.e. what was seen for the higher intensities in this experiment (Latu 2007).

Due to the special features of the LUPIN, the signal can be acquired and saved in a graphical form over a time that can be set by the user. It was then decided to extend the acquisition window up to 100 ms to cross-check the time distribution with the one predicted by FLUKA simulations. The signal acquired over a window of 100 ms is shown in Fig. 8.

If one compares the LUPIN signal with Fig. 5 it can be seen that the time distribution as simulated by FLUKA is completely coherent with what was observed experimentally. After a first very intense part of the signal that is generated in the detector in the first 2 ms, the intensity progressively decreases, until the last neutrons are detected 100 ms later. When one compares the two figures, it should be taken into account that in Fig. 5 $t = 0$ is the time when the beam impinges on the dump, while in Fig. 8 $t = 0$ corresponds to the detection of the first neutron in the LUPIN. However, the time needed by the first neutron to reach the detector after the beam has hit the dump is negligible, i.e. about 2 μs according to the FLUKA simulations.

5. Conclusions

The work described in this paper allowed the study of the linearity of the response to PNF of five neutron detectors up to extreme stray field intensities. The special characteristics of the HiRadMat facility allowed the detectors to be tested in the stray field generated by a proton beam with tuneable intensity impinging on the dump. The stray field was only due to neutrons and this allowed focussing the attention on the analysis of the response, neglecting the problems related to the photon rejection. The primary beam intensity, the stray field intensity and therefore the expected H*(10) per burst could be varied over more than three orders of magnitude. Moreover, the presence of a significant delayed neutron component enabled the detectors to be tested in a pulsed stray field in which a slow contribution is also observed, i.e. in a radiation environment similar to that found in operational conditions.

According to the performance of the detectors, several conclusions can be drawn:

- the gas-filled (Hydrogen or Argon) ionization chambers used in the RAMSES monitoring system at CERN show a quasi-linear response, very close to the ideal behaviour, up to extreme values of H*(10) per burst that could be obtained in the experiment;
- the Wendi-2 and the BIOREM responses are characterized by a strong deviation from the linearity, especially noticeable in the Wendi-2, when the expected H*(10) per burst is higher than a few tens of nSv;
- the LUPIN response shows a slight deviation from the ideal curve for expected values of H*(10) higher than 100 nSv. The deviation becomes rather strong for the extreme beam intensities tested, but this device is nonetheless a very good candidate as both a portable and installed monitor at particle accelerator facilities where a strongly pulsed neutron component is present.

Acknowledgements

The authors wish to thank Ilias Efthymiopoulos for his overall support and for useful technical discussions, and Kurt Weiss and Dino De Paoli for their technical help during the installation and during the measurements. The authors are indebted to Frederic Loprete for his meticulous work in the construction of the aluminium support under a tight time schedule. The authors also wish to thank Doris Forkel-Wirth for her continuous support in this experimental activity. This experiment was partially funded by EuCARD Transnational Access HiRadMat@SPS. This research project has been also supported by a Marie Curie Early Initial Training Network Fellowship of the European Community's Seventh Framework Programme under contract number PITN-GA-2011-289198-ARDENT.

References

Aza, E., Caresana, M., Cassell, C., Charitonidis, N., Harrouch, E., Manessi, G.P., Pangallo, M., Perrin, D., Samara, E., Silari, M., 2013. Instrument Intercomparison in the Pulsed Neutron Fields at the CERN HiRadMat Facility. CERN. Technical Note CERN-RP-2013-037-REPORTS-TN.

Astier, P., Autiero, D., Baldisseri, A., Baldo-Ceolin, M., Banner, M., Bassompierre, G., Benslama, K., Besson, M., Bird, I., Blumenfeld, B., 2003. Prediction of neutrino fluxes in the NOMAD experiment. Nucl. Instrum. Meth. A 515, 800–828.

Battistoni, G., Muraro, S., Sala, P.R., Cerutti, F., Ferrari, A., Roesler, S., Fasso, A., Ranft, J., 2007. The FLUKA code: description and benchmarking. In: Proceedings of the Hadronic Shower Simulation Workshop, Batavia, USA, 6–8 September 2006, AIP Conference Proceeding, vol. 896, pp. 31–49.

Bohm, J., 1976. Saturation corrections for plane-parallel ionization chambers. Phys. Med. Biol. 21, 754–759.

Caresana, M., Denker, A., Esposito, A., Ferrarini, M., Golnik, N., Hohmann, E., Leuschner, A., Luszik-Bhadra, M., Manessi, G.P., Mayer, S., Ott, K., Röhrich, J., Silari, M., Trompier, F., Wielunski, M., 2014. Intercomparison of radiation protection instrumentation in a pulsed neutron field. Nucl. Instrum. Meth. A 737, 203–213.

Caresana, M., Ferrarini, M., Manessi, G.P., Silari, M., Varoli, V., 2013a. LUPIN, a new instrument for pulsed neutron fields. Nucl. Instrum. Meth. A 712, 15–26.

Caresana, M., Ferrarini, M., Manessi, G.P., Silari, M., Varoli, V., 2013b. A neutron detector for pulsed mixed fields: preliminary measurements. In: Proceedings of the 12th International Conference on Radiation Shielding, Nara, Japan, 2–7 September 2012, published in Progress in Nuclear Science and Technology (in press-c).

Charitonidis, N., Efthymiopoulos, I., Theis, C., Vincke, H., 2011. Prompt, Activation and Background Radiation Studies for the HiRadMat Facility of CERN/SPS. CERN. Technical Note, EDMS No. 1144976.

Charitonidis, N., Manessi, G.P., Silari, M., 2012. Test Run for the HRMT-15 (RPNIST) Experiment. CERN. Technical Note CERN-DGS-2012-092-RP-TN.

Charitonidis, N., Harrouch, E., 2013. Round Detector Support for HRM-15 (RPINST) Experiment. CERN. Technical Note, EDMS No. 1249864.

Efthymiopoulos, I., Hessler, C., Gaillard, H., Grenier, D., Meddahi, M., Trilhe, P., Pardons, A., Theis, C., Charitonidis, N., Evrard, S., Vincke, H., Lazzaroni, M., 2011. HiRadMat: a new irradiation facility for material testing at CERN. In: Proceedings of IPAC 2011, San Sebastian, Spain, 4–9 September 2011. TUPS058.

Fasso, A., Ferrari, A., Ranft, J., Sala, P.R., 2005. FLUKA: a Multi-particle Transport Code. CERN. Technical Note, CERN-2005-10, INFN/TC_05/11, SLAC-R-773.

Ferrarini, M., Varoli, V., Favalli, A., Caresana, M., Pedersen, B., 2010. A wide dynamic range BF_3 neutron monitor with front-end electronics based on a logarithmic amplifier. Nucl. Instrum. Meth. A 613, 272–276.

Grenier, D., Pardons, A., 2011. TED-type Beam Dump. CERN. Technical Note, EDMS No. 1145913.
Jägerhofer, L., Feldbaumer, E., Theis, C., Roesler, S., Vincke, H., 2012. A new method to calculate the response of the Wendi-2 rem counter using the FLUKA Monte Carlo code. Nucl. Instrum. Meth. A 691, 81–85.
Knoll, G.F., 2010. Radiation Detection and Measurement, fourth ed. John Wiley & Sons Inc, pp. 124–126.
Latu, M., 2007. Radiation Monitoring System for the Environment and Safety. CERN. Technical Note (in French), EDMS No. 770397.
Olsher, R.H., Hsu, H.H., Beverding, A., Kleck, J.H., Casson, W.H., Vasilik, D.G., Devine, R.T., 2000. Wendi: an improved neutron rem meter. Health Phys. 79, 170–181.
Olsher, R.H., McLean, T.D., 2008. High-energy response of the PRESCILA and Wendi-II neutron rem meters. Rad. Prot. Dosim. 130, 510–513.
Rios, I., Gonzalez, J., Mayer, R.E., 2013. Total fluence influence on the detected magnitude of neutron burst using proportional detectors. Rad. Meas. 53–54, 31–37.
Segura Millan, G., Perrin, D., Scibile, L., 2006. RAMSES: the LHC radiation monitoring system for the environment and safety. In: Proceedings of the 10th International Conference on Accelerator & Large Experimental Physics Control Systems, Geneva, Switzerland, 10–14 October 2005. TH3B.1-3O.
Theis, C., Rettig, M., Roesler, S., Vincke, H., 2004. Simulation and Experimental Verification of the Response Functions of Centronic High-pressure Ionisation Chambers. CERN. Technical Note, CERN-SC-2004-23-RP-TN.
Theis, C., 2007. The Radiation Environment in Underground Workplaces of the LHC. PhD thesis. Graz University of Technology (Chapter 2).
Thermo Scientific FHT 725/FHT 752 H User's Manual, Version 28.02.2008.